


Low Threshold Polariton Lasing from a Solution-Processed Organic Semiconductor in a Planar Microcavity

Sai Kiran Rajendran, Mengjie Wei, Hamid Ohadi, Arvydas Ruseckas, Graham A. Turnbull,* and Ifor D. W. Samuel*

Organic semiconductor materials are widely studied for light emission and lasing due to their ability to tune the emission wavelength through chemical structural modification and their relative ease of fabrication. Strong light–matter coupling is a promising route toward a coherent light source because it has the potential for polariton lasing without population inversion. However, the materials studied so far have relatively high thresholds for polariton lasing. Here, the suitability of pentafluorene for strong coupling and low threshold polariton lasing is reported. A protective buffer layer is used to reduce degradation during fabrication and the lasing threshold is lowered using negative detuning to maximize radiative decay. A low threshold of $17 \mu\text{J cm}^{-2}$, corresponding to an absorbed energy density of $11.7 \mu\text{J cm}^{-2}$, is obtained. This study shows that pentafluorene is an attractive material for polariton lasing and will assist in the development of low threshold electrically pumped lasing from polariton devices.

Strongly coupled light–matter systems have attracted considerable interest due to their possibility to realize low threshold polariton lasing as well as to study quantum systems such as polariton condensation and superfluidity.^[1] Only a few inorganic semiconductor materials that exhibit high binding energy have demonstrated room-temperature low threshold polariton lasing.^[2] Organic semiconductor materials can show robust strong coupling at room temperatures,^[3] due to their large exciton binding energy (of several hundreds of meV) and high oscillator strength. They have been widely applied in light-emitting devices and conventional lasers,^[4] but despite these promising features, it is only recently that polariton lasing has been realized in such materials.^[5,6] A growing understanding of the suitability of organic semiconductor materials is now opening up more detailed studies of polariton condensates, including lateral confinement, studies of coherence, stability, and superfluidity.^[7,8]

Dr. S. K. Rajendran, M. Wei, Dr. H. Ohadi, Dr. A. Ruseckas,
Prof. G. A. Turnbull, Prof. I. D. W. Samuel
Organic Semiconductor Centre
SUPA
School of Physics and Astronomy
University of St Andrews
St Andrews KY16 9SS, UK
E-mail: gat@st-andrews.ac.uk; idws@st-andrews.ac.uk

 The ORCID identification number(s) for the author(s) of this article can be found under <https://doi.org/10.1002/adom.201801791>.

DOI: 10.1002/adom.201801791

A major attraction of polariton lasers is the potential to achieve much lower thresholds than in conventional photon lasers, since no population inversion is required. Achieving low threshold operation is vital for future organic polariton devices, both to enhance stability by reducing photoinduced degradation and to reduce the number of charge carriers required to achieve an electrically pumped polariton laser. However, the cavity polariton lasing thresholds from organic semiconductors in planar microcavities reported to date^[5,6] are higher than $300 \mu\text{J cm}^{-2}$ in incident excitation density and also higher than photon lasing thresholds from the same class of materials. There is therefore a need for new materials that can achieve low threshold polariton lasing.

In this paper, we report polariton lasing using an oligofluorene in a planar dielectric microcavity giving an order of magnitude reduction in threshold to $17 \mu\text{J cm}^{-2}$. This corresponds to an absorbed energy density of $11.7 \mu\text{J cm}^{-2}$. It is also comparable with the lowest plasmon exciton polariton lasing threshold of $18 \mu\text{J cm}^{-2}$, obtained from a dye on a laterally patterned nanoparticle array.^[9]

To achieve this low-threshold operation, we select a material with high photoluminescence quantum yield (PLQY) and oscillator strength, pentafluorene, and introduce a buffer layer in the top mirror to retain the high PLQY in the dielectric microcavity. We observe the key features of polariton lasing including a nonlinear emission intensity beyond a threshold excitation density, a drop in the spectral linewidth of emission, and increase in directionality of emission. An associated collapse in the spatial distribution of emission and macroscopic coherence are also observed. In contrast with photon lasing, accumulation of population is at the bottom of the lower polariton branch. We also observe a drop in polariton lasing threshold by simultaneously increasing the radiative component of the lower polariton mode through negative detuning and the proximity to the spectral gain window of pentafluorene. This suggests that the population mechanism dominating the lower polariton branch is largely radiative.^[10]

Oligofluorenes are a class of materials associated with high exciton binding energy and absorption oscillator strength.^[11,12] They are also associated with very short radiative lifetimes^[11,13] and high photoluminescence (PL) quantum yield.^[14] Oligofluorene films have been reported not to show green excimer

emission when annealed in air as can happen in polymers.^[13] Oligofluorene films have also shown amplified spontaneous emission^[15] with thresholds of the order of $1 \mu\text{J cm}^{-2}$. Oligofluorenes can be easily synthesized and processed into films from solution or evaporated to give films of a desired thickness. These properties make oligofluorenes suitable materials for organic polariton lasers. In a previous study, we observed that the PLQY increased and the radiative lifetime decreased when the number of fluorene units in oligofluorene increases.^[14] The transition dipole moment also increased with the oligomer length. For these reasons, we chose to study pentafluorene in this work.

Pentafluorene has an inhomogeneously broadened absorption peak at 369 nm (3.36 eV) with a full width at half maximum (FWHM) of 60 nm (517 meV). The emission from neat films presents two vibronic peaks at 417 nm (2.96 eV) and 442 nm (2.81 eV) with an overall FWHM of 44.5 nm (314 meV). The energy difference between the peak absorption and peak emission is 400 meV. The neat films also present a very short emission lifetime of 440 ps and a high PLQY close to 90% (see the Supporting Information for more details). We fabricate strongly coupled pentafluorene in planar microcavities by spin-coating neat films of different thicknesses sandwiched between distributed Bragg reflectors (DBRs) (Figure 1a). The DBRs consisted of pairs of $\text{SiO}_2/\text{Ta}_2\text{O}_5$ and were designed with a center reflectivity of 410 nm (3.02 eV) at normal incidence to include both the peak absorption and the two main emission peaks within the stop band (Figure 1b). The bottom DBR bandwidth was also optimized to have peak transmission at 343 nm (3.62 eV) to allow optimal excitation of the pentafluorene by the 343 nm laser pulses incident on the bottom DBR. The deposition of the top DBR by radiofrequency (RF) sputtering on pentafluorene would expose the active material to argon and oxygen plasma. Studies on cellulose and polypropylene have shown that cleavage and oxidation of covalent bonds in the organic materials up to 10 nm from the surface can take place on exposure to RF argon and oxygen plasma.^[16] Such functionalization would degrade the light-emitting properties of pentafluorene. Hence, there is a need to protect the active material using a transparent material with a thickness of about 10 nm. While sputtering cannot be used to deposit the protective layer, spin-coating is also unsuitable

at it would dissolve the active material. Lithium fluoride (LiF) was chosen as an appropriate material that can be evaporated to about 10 nm thickness on pentafluorene films. We find that sputter deposition on bare pentafluorene reduces the PLQY to 34%, but a LiF protective layer followed by a sputtered layer gives a PLQY of the pentafluorene of 56% (see Section S1, Supporting Information). The bottom (top) DBRs showed a transmission minimum of 0.8% (1.8%). Using values of 99.2% (98.2%) for reflectivity, we calculate a finesse of 290 for the cavities.

Three cavities A, B, and C were fabricated with neat pentafluorene active layer films of different thicknesses resulting in polariton modes at 437, 432, and 422 nm, respectively, at normal incidence. The thicknesses of the films in the three cavities were estimated to be 115, 110, and 94 nm, respectively, based on transfer matrix calculations of the cavity resonance. Test films deposited under similar conditions later resulted in films between 105 and 76 nm for similar range of spin speeds. The optical resonances are negatively detuned from the exciton energy at normal angle of incidence. Experimental measurement of the angle-dependent reflectivity from cavity A is shown using scattered points in Figure 1c. The experimentally recorded reflectivity spectra at small and large angles are shown in Section S2 (Supporting Information). An anticrossing in the dispersion, a characteristic feature of strong coupling, is clearly observed. The dispersion of the lower and upper polariton modes can be matched to a coupled oscillator model whose solutions follow the relation

$$E_{U,L}(\theta) = \left[(E_p(\theta) + E_{ex}) \pm \sqrt{(E_p(\theta) - E_{ex})^2 + 4\Omega^2} \right] / 2 \quad (1)$$

for the energy of the upper (E_U) and lower polariton (E_L) modes, where $E_{ex} = 3.4$ eV is the peak absorption energy of pentafluorene film, $E_p(\theta)$ is the angle (θ) dependent energy of the cavity mode given by

$$E_p(\theta) = E_p(0) / \sqrt{1 - \frac{\sin^2\theta}{n_{\text{eff}}^2}} \quad (2)$$

$n_{\text{eff}} = 1.8$ is the effective refractive index of the cavity, giving a half-Rabi splitting energy (Ω) of ≈ 250 meV. The coupled

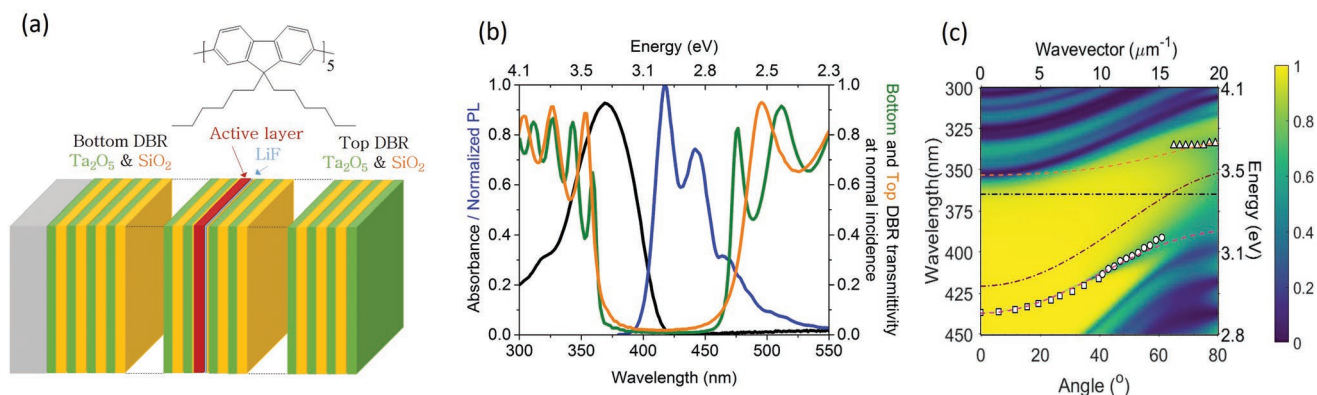


Figure 1. a) Structure of pentafluorene, and sketch of the planar microcavity. b) Absorption (black), steady state emission (blue) spectra of a neat pentafluorene film, and transmission spectra through the sputtered bottom (green) and top (orange) reference DBRs at normal incidence. c) Transfer matrix calculated spectra in pseudo color plots, the experimental reflectivity minima of the lower and upper polariton branch from cavity A as scatter plots, and matching coupled oscillator model dispersion as dashed lines are depicted.

oscillator model dispersion is plotted with dotted lines in Figure 1c. The dispersion of the pentafluorene microcavities was also calculated using transfer matrix approach. The refractive index of neat pentafluorene film was obtained using fits to experimentally recorded variable angle spectroscopic ellipsometry (see Figure S4, Supporting Information). The TM polarized reflectivity of the cavity was then calculated for a 115 nm thick active layer as shown in Figure 1c as pseudo color map. Both methods fit excellently with the experimental data. From the coupled oscillator model, the photon fraction of the polariton mode and detuning (energetic separation between the exciton and photon mode) can be extracted (see Figure S5, Supporting Information). We have 85 to 75% photon fraction at the bottom of the lower polariton branch and a negative detuning of 450, 400, and 330 meV for the three cavities.

To measure the lasing characteristics of the pentafluorene microcavities, the angle-resolved polariton emission spectra were recorded in Fourier space by varying the excitation density.^[17] The cavities were excited nonresonantly with 343 nm, 200 fs duration pulses through the substrate. **Figure 2a–c** depicts the vertically polarized emission from cavity A at three different incident (absorbed) excitation densities of $0.5 P_{th}^A$, $1.5 P_{th}^A$, and $3 P_{th}^A$ where $P_{th}^A = 16.7$ (11.7) $\mu\text{J cm}^{-2}$ (4.0 nJ pulse energy, 175 μm spot diameter). Below threshold the emission follows the lower polariton dispersion obtained in the reflectivity spectra with emission over a large range of angles (Figure 2a). The cavity

mode obtained from the coupled oscillator model is plotted as yellow dashed lines. The uncoupled dispersionless pentafluorene film emissions at 417 and 442 nm (vibronic peaks) are weak showing the consistency and quality of the fabrication. The absence of these features below threshold indicates that the molecules are strongly coupled and emission occurs only through the polariton mode. Above threshold a spectrally narrow and highly directional emission from the bottom of the lower polariton branch appears, which increases in intensity rapidly with increasing excitation density (Figure 2b). This is a key feature of polariton lasing where polaritons of large in-plane wave vector ($k_{||}$) accumulate macroscopically at the bottom of the lower polariton branch. We note that the emission has a narrow divergence and flat dispersion suggesting that it comes from a spatially localized state at a single energy. At $3 P_{th}^A$, the emission extends to higher energy modes due to repulsive interaction between polaritons (Figure 2c) similar to inorganic microcavities.^[18]

Real space images of the emission show the localization effect as intensity increase. At $0.5 P_{th}^A$ the emitting spot has the same size as the excitation spot showing a Gaussian distribution of polariton emission (Figure 2d). As the threshold is crossed the peak emission emerges mainly from localized spots extending a few micrometers in size, as seen in many other materials^[7] (Figure 2e). The positions of the spots are repeatable with measurements of the same excitation densities showing

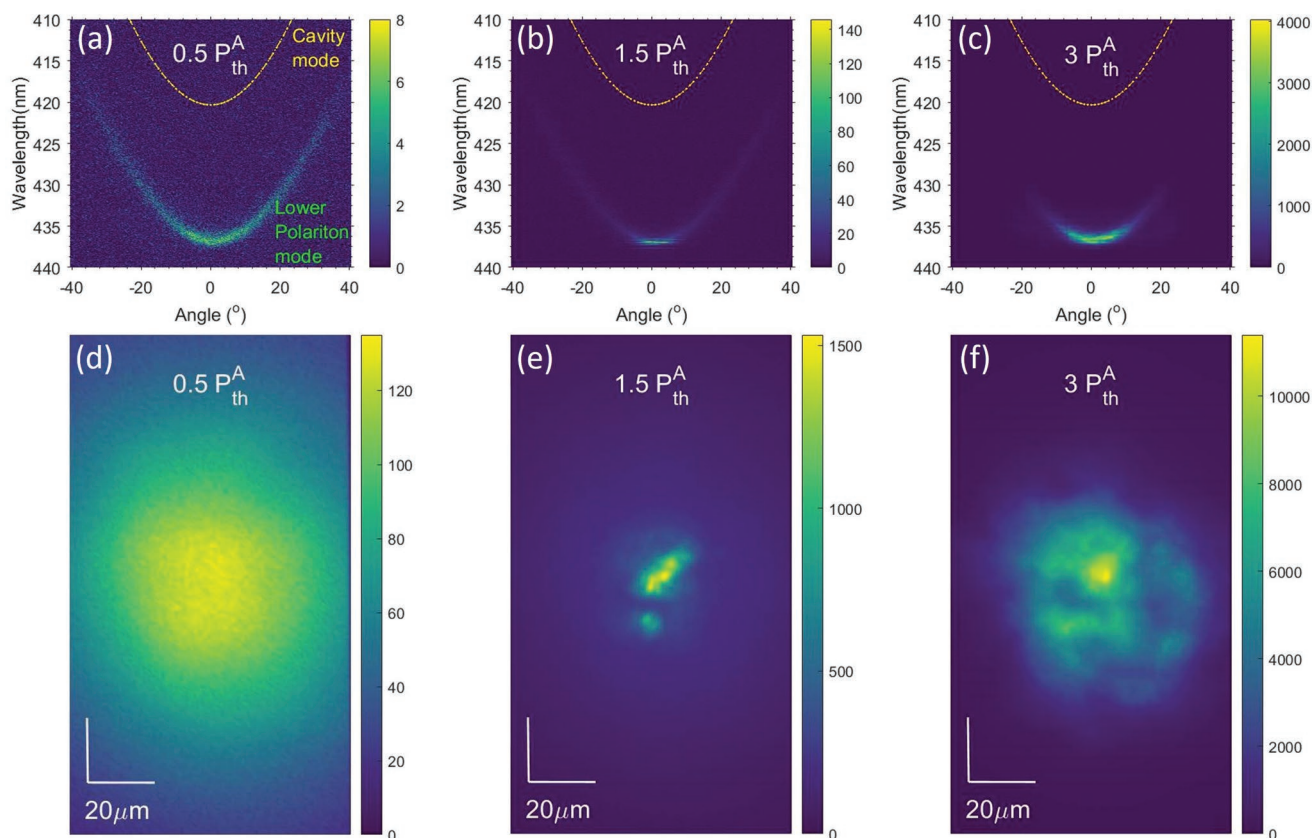


Figure 2. a–c) Angle-resolved lower polariton emission from cavity A, with incident (absorbed) threshold excitation density (P_{th}^A) of $16.7 \mu\text{J cm}^{-2}$ ($11.7 \mu\text{J cm}^{-2}$) with estimated cavity mode as dotted lines. The emission dispersion a) below threshold, b) above threshold, and c) at $3 P_{th}^A$. d–f) Corresponding real space distribution of emission.

that they may be due to inhomogeneity in the film thickness. On increasing the excitation density further the lasing spots spread to a larger area as a result of polariton repulsive interactions (Figure 2f).

Cavities B and C show similar emission spectra (see Figure S6, Supporting Information). However, the incident (absorbed) lasing threshold increases as the detuning reduces giving $P_{th}^B = 20 \mu\text{J cm}^{-2}$ ($14 \mu\text{J cm}^{-2}$) and $P_{th}^C = 46 \mu\text{J cm}^{-2}$ ($32.2 \mu\text{J cm}^{-2}$). This could be attributed to higher losses due to reabsorption of excitations by the uncoupled exciton reservoir, as increasing the cavity frequency leads to greater overlap with the molecular absorption spectrum. Despite this, polariton lasing is observed over a wide range of negative detunings in these cavities. The uncoupled exciton reservoir can in principle decay both radiatively as well as nonradiatively into the lower polariton branch.^[10] Strongly coupled J-aggregates have been observed to decay predominantly nonradiatively^[19] due to their low PLQY. However, drop in polariton lasing threshold with the larger PLQY pentafluorene and larger detuning suggest that radiative decay is the dominant polariton relaxation mechanism here. From real space images in both these cavities (Figure S6d–f and j–l, Supporting Information), it is observed that below threshold the spatial polariton distribution follows the excitation spot. Above threshold excitation density, highly populated regions

that are spatially fragmented and localized near the excitation spot center appear. With increasing excitation density, polariton repulsive interaction that results in blueshifted emission also results in spatial spread to a larger area.

Figure 3a shows several emitted spectra, collected in the range of $\pm 5^\circ$ (or $|k_{||}| < 1.3 \mu\text{m}^{-1}$), above and below threshold excitation density (P_{th}^A) for cavity A. We observe that sharp intense peaks appear above threshold that do not shift in energy. At threshold, a narrow peak on the low energy side of the lower polariton branch emerges and increases in intensity with excitation density. Above threshold multiple narrow peaks each of spectral FWHM around 0.2 nm emerge. We believe that the disorder in layer thickness across the sample leading to variation in resonant photon energy, is the reason for multiple peaks in the emission spectrum above threshold. Figure 3b plots the peak emission intensity as a function of incident excitation density (solid symbols). Below threshold the peak intensity increases sublinearly while above the threshold excitation density, the emitted intensity increases superlinearly. For the range of excitation densities up to $3P_{th}^A$ the emission is repeatable as seen through three consecutive measurements. A second threshold into photon lasing regime was not observed as the cavity undergoes irreversible photodegradation of emission intensity for excitation densities beyond $3P_{th}^A$. For organic

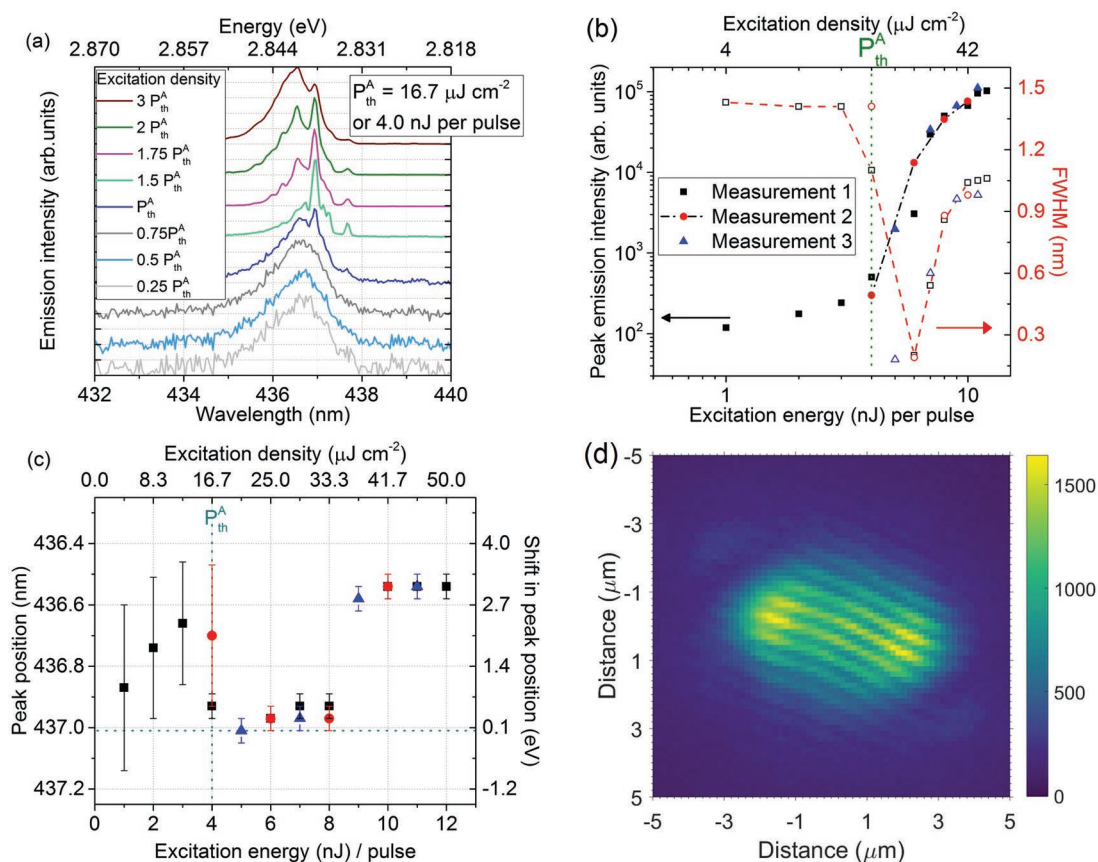


Figure 3. a) Normalized and vertically translated emission spectra from cavity A collected in the range of $\pm 5^\circ$ with change in excitation density. b) Peak emission intensity (solid symbols) from cavity A shows nonlinearity with excitation density and drop in spectral FWHM (hollow symbols) at threshold. c) Peak emission wavelength from cavity shows an initial redshift at threshold followed by a blueshift with increasing polariton density. d) An interferogram at $26 \mu\text{J cm}^{-2}$ incident excitation density showing long-range spatial coherence in cavity A.

semiconductors in planar microcavities, only green fluorescent protein has been able to show this transition at an excitation density of about 250 mJ cm^{-2} (125 nJ on $8 \text{ }\mu\text{m}$ spot) due to its high damage threshold.^[5] The spectral FWHM over this angular range of emission is plotted in the same graph using hollow symbols. The emission linewidth at normal incidence below threshold is 1.4 nm (9.8 meV). Just above threshold the FWHM drops to 0.2 nm (1.4 meV). With increasing excitation density, due to simultaneous population of narrow modes, the effective FWHM increases. The blueshift of peak spectral emission is an indication of repulsive interaction between polaritons (Figure 3c). The blueshift below threshold is negligible compared to the spectral FWHM and hence can be neglected. At threshold, there is a small redshift of peak emission as a result of multiple narrow peaks appearing within the lower polariton mode possibly due to disorder in cavity thickness across the excitation spot. At higher excitation densities, the relative intensities of the multiple narrow peaks change showing an effective blueshift of 3 meV . While the shift is smaller than the effective FWHM due to the multiple modes, it is of similar magnitude to that observed in other organic semiconductor polariton lasers.^[5–8] However, each of the narrow peaks do not shift significantly in energy, indicating weak polariton–polariton interactions.

Similar spectra emitted from cavity B and C are presented in Figure S7 (Supporting Information). Below threshold the emission from these cavities has a slightly larger spectral FWHM possibly due to increased inhomogeneity in the film. We also see that above threshold the line shape appears to consist of multiple sharp lines. Once again, each of these narrow modes has a spectral FWHM of about 0.2 nm . However, simultaneous population of these modes results in larger effective spectral FWHM. Both the cavities exhibit lasing from the bottom of the lower polariton branch above threshold followed by an effective blueshift of the peak position by about 3 meV . The pump energy dependence of the emission intensity is repeatable about the threshold excitation density for all the three cavities.

It was also observed that the polariton emission below threshold was largely unpolarized. The cavities were pumped nonresonantly with respect to the lower polariton branch or bottom of the exciton reservoir in order to allow polarization memory loss. However, polariton emission above threshold excitation density had the same polarization as the pump laser. This is due to the scattering rate into the bottom of the lower polariton branch at high excitation densities being much faster than the depolarization time. Details of polariton emission polarization with different pump polarization are given in Section S6 (Supporting Information). Similar polarization pinning has been observed in MeLPPP cavities by Plumhof et al.^[5]

Long-range coherence is another indicator of polariton lasing. In order to demonstrate the appearance of long-range coherence, emission from the sample was split in a Mach-Zehnder interferometer with a retroreflector in one arm and interfered spatially and temporally onto a CCD to acquire an interferogram.^[18] Figure 3d shows an interferogram when cavity A is excited above threshold density. Fringes are visible up to $5 \text{ }\mu\text{m}$ in distance showing that long-range spatial coherence is present (see Section S7, Supporting Information, for

more details). All three cavities show onset of fringes only above threshold excitation density. These fringes are absent below threshold excitation density showing that coherence is not forced on polariton emission by the excitation pulses themselves. We find that similar to inorganic microcavities multiple spatially separated condensates can appear which then phase-lock as excitation power is increased.^[20] The results provide clear evidence of macroscopic coherence from the emitting spots.

In conclusion, pentafluorene was identified as a promising material for room-temperature polaritonics. In particular, it was found to give strong coupling and low threshold polariton lasing due to its strong absorption as well as high PLQY. Our results are compared with thresholds of other cavity polariton lasers in Table 1. The table shows the thresholds of organic and inorganic semiconductor materials that have been reported to show room-temperature polariton lasing in microcavities. Among organic materials, pentafluorene has the lowest incident excitation threshold by an order of magnitude and is less than half of the lowest reported absorbed energy density. Inorganic semiconductor materials also present a comparable low threshold but generally require more complex fabrication techniques. It may be possible to reduce the polariton lasing threshold further in pentafluorene by either optimizing the protective layer or changing the photonic confinement geometry to a 0D cavity or a surface plasmon coupled structure. In this work, we showed that the active layer can be deposited by spin-coating and that by using an appropriate protective layer, a top DBR can be sputter deposited without significant degradation. Strong coupling in pentafluorene cavities was achieved exhibiting a Rabi splitting energy of 500 meV . Low threshold polariton lasing was achieved in three differently detuned pentafluorene cavities. It was observed that the threshold reduces in cavities with larger negative detuning and this was assigned to be due to a higher radiative decay component of the polariton mode. On excitation with a large spot, we see fragmentation into several bright spots. They are found to be coherent with each other even though separated by a few micrometers distance. This study significantly lowers the polariton lasing thresholds demonstrated so far with strongly coupled organic semiconductors in planar microcavities and so brings electrical pumping of such devices closer.

Experimental Section

The absorption spectrum of the pentafluorene film was recorded with a UV–visible spectrometer CARY 300 and steady-state PL spectrum was recorded using an Edinburgh Instruments FLS 980 fluorimeter with 343 nm excitation from a Xenon lamp. The complex refractive index of pentafluorene film was determined by spin-coating the film on a silicon substrate and performing variable angle spectroscopic ellipsometry. Using WVASE32 software the data were first fitted in the transparent region to determine the parameters for a Cauchy model. These parameters were then fixed and a multiple regression fit was performed to obtain the complex refractive index of the film over the entire range of the UV–visible spectrum.

The DBR mirrors were RF sputter deposited in an Angstrom Engineering deposition system. Alternating layers of 46.5 nm Ta_2O_5 and 69.7 nm SiO_2 , 10.5 pairs in total, followed by 10 nm SiO_2 were sputtered on quartz substrates, to fabricate the bottom DBR. Pentafluorene,

Table 1. Summary of room-temperature microcavity polariton lasing thresholds from strongly coupled organic and inorganic semiconductor materials.

Active semiconductor material		Planar microcavity structure for strong coupling	Lasing threshold energy density	
			Incident	Absorbed
Organic	Pentafluorene (present work)	10.5 pairs of alternating Ta ₂ O ₅ and SiO ₂ layers for bottom DBR and 6.5 pairs for top DBR. 105 nm thick active layer is spin-coated and protected on top with evaporated 10 nm thick LiF layer and another 10 nm thick SiO ₂ sputtered layer.	17 μJ cm ⁻²	12 μJ cm ⁻²
	MeLPPP ^[7b]	Plano-concave 0D cavity (planar cavity with 30 μm deep Gaussian defect on top mirror) with 9.5 and 6.5 pairs of alternating Ta ₂ O ₅ and SiO ₂ layers for bottom and top DBRs. Active material is 35 nm thick with 10 nm thick protective SiO ₂ layer sputtered on top in a tunable open cavity.	130 μJ cm ⁻²	
	Bodipy dye ^[5d]	Ten and eight pairs of alternating SiO ₂ and Nb ₂ O ₅ layers for bottom and top DBRs. Active layer thickness is 186 nm.	527 μJ cm ⁻²	
	eGFP ^[5c]	Identical 14 pairs of alternating SiO ₂ and Ta ₂ O ₅ layers for bottom and top DBRs. Active material is 500 nm thick in a 1.5–4.5 μm thick tunable open (laminated) cavity.	24 000 μJ cm ⁻²	
	TDAF ^[6,7c]	Identical nine pairs of alternating SiO ₂ and Ta ₂ O ₅ layers for bottom and top DBRs. Active material is 120 nm thick.	600 μJ cm ⁻²	27 μJ cm ⁻²
	MeLPPP ^[5b]	9.5 and 6.5 pairs of alternating Ta ₂ O ₅ and SiO ₂ layers for bottom and top DBRs. 35 nm thick active material is sandwiched between 50 nm thick buffer SiO ₂ layers.	500 μJ cm ⁻²	
Inorganic	Anthracene single crystals ^[5a]	Identical 12 pairs of alternating SiO ₂ and SiN _{1.94} layers for bottom and top DBRs. Crystals in active layer were formed in 120 nm thick channels.		320 μJ cm ⁻²
	CsPbCl ₃ perovskite nanoplatelets ^[2e]	13 and 7 pairs of HfO ₂ /SiO ₂ layers for the bottom and top DBRs, respectively. Active layer is 373 nm thick.	12 μJ cm ⁻²	
	ZnO ^[2d]	30 pairs of AlN/Al _{0.23} Ga _{0.77} N layers for the bottom DBR and 9 pairs of SiO ₂ /HfO ₂ layers for the top DBR. 3λ/2 thick active layer is used.	31.8 kW cm ⁻²	
	GaN nanowire ^[2c]	Identical seven pairs of SiO ₂ and TiO ₂ layers for the bottom and top DBRs. Nanowires embedded in a λ cavity	93 nJ cm ⁻²	
	GaN/AlGaN multiple quantum wells ^[2b]	35 pairs of Al _{0.85} In _{0.15} N/Al _{0.2} Ga _{0.8} N layers for bottom DBR and 13 pairs of SiO ₂ /Si ₃ N ₄ layers for the top DBR. Active layer consists of GaN/Al _{0.2} Ga _{0.8} N quantum wells forming a 3λ cavity structure.	17.7 W cm ⁻²	
	GaN ^[2a]	35 pairs of Al _{0.85} In _{0.15} N/Al _{0.2} Ga _{0.8} N layers for bottom DBR and 10 pairs of SiO ₂ /Si ₃ N ₄ layers for the top DBR. Active layer is 210 nm thick forming a 3λ/2 structure.		27 μJ cm ⁻²

purchased from American Dye Source Inc. ADS056FO, was dissolved in toluene (99.8% anhydrous, Sigma Aldrich) at a concentration of 22 mg mL⁻¹ and left stirring overnight at 323 K. It was then sonicated in an ultrasonic bath for 1 min and spin-coated on the DBRs. A range of spin speeds were used to form films of different thicknesses in a nitrogen glove box environment. The thickness of the active layer in the cavities was estimated using spectroscopic ellipsometric measurements of similarly deposited films on glass substrates. A 10 nm thick LiF layer was then evaporated on the organic film to protect it from plasma during subsequent top DBR sputtering process. The top DBR consisted of 10 nm SiO₂ followed by 6.5 pairs of alternating 46.5 nm Ta₂O₅ and 69.7 nm SiO₂.

Angle-resolved reflectivity spectra for angles from 0° to 40.5° were measured using Fourier plane imaging with a 0.65 numerical aperture Nikon microscope objective onto the slit of a spectrometer (Andor 500SR coupled to an IDus 420 CCD or Newton 940 CCD). The angle-resolved reflectivity in the range of 42°–75° was recorded using a J. A. Woollam VASE ellipsometer with the white light focused on to a 200 μm diameter spot. For polariton lasing studies, 200 fs duration pulses of 343 nm wavelength generated from the third harmonic of a femtosecond laser (Pharos from Light Conversion) were focused on the microcavities using a 250 mm focal length lens from the substrate side. The emission was collected using the Nikon objective from the top DBR side and angle resolved again by Fourier plane imaging. The real space images of the emitting spot were also recorded on the same CCD spectrometer with the zeroth order of the grating. The excitation spot size was measured using a beam profilometer (Lasercam HR from Coherent) to be 175 μm at the sample plane. The magnification of the real space imaging system was estimated using a Thorlabs high resolution target (R2L2S1N1). For lasing studies, the incident excitation density was varied using a neutral

density filter and the averaged incident energy per pulse was calculated using the average excitation power measured using a photodiode sensor head (Thorlabs S170C coupled to PM100D console) and repetition rate. The angle-resolved emission was collected by the Andor spectrograph at each excitation density for 0.5 s with the excitation repetition rate at 5 or 1 kHz.

For macroscopic coherence measurements, reflection geometry was used for excitation and emission detection with a Nikon 0.65 numerical aperture objective in order to create a small number of closely spaced lasing spots. The collected emission was split into two arms of an interferometer that directed the reflected and retroreflected image into the Andor CCD spectrograph.

Supporting Information

Supporting Information is available from the Wiley Online Library or from the author. The data that support the findings of this study are openly available in St Andrews research portal at <http://doi.org/10.17630/5503c28f-dea7-4a6e-afca-a6a2e89275d3>.

Acknowledgements

The authors are grateful to EPSRC for support through the Hybrid Polaritonics program grant (EP/M025330/1). The authors are also thankful to Jonathan Keeling, University of St Andrews, for useful discussions toward the interpretation of the results. S.K.R. acknowledges valuable help from Laura Tropic, University of St Andrews, regarding

sputter deposition and Simon Betzold, Christof Dietrich, and Sven Höfling, Universität Würzburg, for support with the experimental setup.

Conflict of Interest

The authors declare no conflict of interest.

Keywords

low threshold, microcavities, organic semiconductors, polariton lasing, strong coupling

Received: December 22, 2018

Revised: March 15, 2019

Published online:

- [1] a) A. Imamoğlu, R. J. Ram, S. Pau, Y. Yamamoto, *Phys. Rev. A* **1996**, 53, 4250; b) H. Deng, H. Haug, Y. Yamamoto, *Rev. Mod. Phys.* **2010**, 82, 1489; c) A. Amo, J. Lefrère, S. Pigeon, C. Adrados, C. Ciuti, I. Carusotto, R. Houdré, E. Giacobino, A. Bramati, *Nat. Phys.* **2009**, 5, 805.
- [2] a) S. Christopoulos, G. B. H. Von Hogerthal, A. J. D. Grundy, P. G. Lagoudakis, A. V. Kavokin, J. J. Baumberg, G. Christmann, R. Butte, E. Feltn, J. F. Carlin, N. Grandjean, *Phys. Rev. Lett.* **2007**, 98, 126405; b) G. Christmann, R. Buttf, E. Feltn, J. F. Carlin, N. Grandjean, *Appl. Phys. Lett.* **2008**, 93, 051102; c) A. Das, J. Heo, M. Jankowski, W. Guo, L. Zhang, H. Deng, P. Bhattacharya, *Phys. Rev. Lett.* **2011**, 107, 066405; d) T.-C. Lu, Y.-Y. Lai, Y.-P. Lan, S.-W. Huang, J.-R. Chen, Y.-C. Wu, W.-F. Hsieh, H. Deng, *Opt. Express* **2012**, 20, 5530; e) R. Su, C. Diederichs, J. Wang, T. C. H. Liew, J. Zhao, S. Liu, W. Xu, Z. Chen, Q. Xiong, *Nano Lett.* **2017**, 17, 3982.
- [3] a) D. G. Lidzey, D. D. C. Bradley, M. S. Skolnick, T. Virgili, S. Walker, D. M. Whittaker, *Nature* **1998**, 395, 53; b) R. J. Holmes, S. R. Forrest, *Org. Electron.* **2007**, 8, 77.
- [4] a) K. Müllen, U. Scherf, *Organic Light Emitting Devices: Synthesis, Properties and Applications*, Wiley, New York **2006**; b) I. D. W. Samuel, G. A. Turnbull, *Chem. Rev.* **2007**, 107, 1272.
- [5] a) S. Kéna-Cohen, S. R. Forrest, *Nat. Photonics* **2010**, 4, 371; b) J. D. Plumhof, T. Stöferle, L. Mai, U. Scherf, R. F. Mahrt, *Nat. Mater.* **2014**, 13, 247; c) C. P. Dietrich, A. Steude, L. Trops, M. Schubert, N. M. Kronenberg, K. Ostermann, S. Höfling, M. C. Gather, *Sci. Adv.* **2016**, 2, e1600666; d) T. Cookson, K. Georgiou, A. Zasedatelev, R. T. Grant, T. Virgili, M. Cavazzini, F. Galeotti, C. Clark, N. G. Berloff, D. G. Lidzey, P. G. Lagoudakis, *Adv. Opt. Mater.* **2017**, 5, 1.
- [6] K. S. Daskalakis, S. A. Maier, R. Murray, S. Kéna-Cohen, *Nat. Mater.* **2014**, 13, 271.
- [7] a) D. Sanvitto, S. Kéna-Cohen, *Nat. Mater.* **2016**, 15, 1061; b) F. Scafirimuto, D. Urbonas, U. Scherf, R. F. Mahrt, T. Stöferle, *ACS Photonics* **2018**, 5, 85; c) K. S. Daskalakis, S. A. Maier, S. Kéna-Cohen, *Phys. Rev. Lett.* **2015**, 115, 1; d) G. Lerario, A. Fieramosca, F. Barachati, D. Ballarini, K. S. Daskalakis, L. Dominici, M. De Giorgi, S. A. Maier, G. Gigli, S. Kéna-Cohen, D. Sanvitto, *Nat. Phys.* **2017**, 13, 837.
- [8] N. Bobrovska, M. Matuszewski, K. S. Daskalakis, S. A. Maier, S. Kéna-Cohen, *ACS Photonics* **2018**, 5, 111.
- [9] M. Ramezani, A. Halpin, A. I. Fernandez-Dominguez, J. Feist, S. R. K. Rodriguez, F. J. Garcia-Vidal, J. G. Rivas, *Optica* **2017**, 4, 31.
- [10] a) M. Litinskaya, P. Reineker, V. M. Agronovich, *J. Lumin.* **2004**, 110, 364; b) P. Michetti, G. La Rocca, *Phys. Rev. B* **2009**, 79, 035325; c) L. Mazza, G. C. La Rocca, *Phys. Rev. B* **2009**, 80, 235314.
- [11] R. Anémian, J.-C. Mulatier, C. Andraud, O. Stéphan, J.-C. Vial, *Chem. Commun.* **2002**, 3, 1608.
- [12] J. Jo, C. Chi, S. Höger, G. Wegner, D. Y. Yoon, *Chem. - Eur. J.* **2004**, 10, 2681.
- [13] C. Chi, C. Im, G. Wegner, *J. Chem. Phys.* **2006**, 124, 024907.
- [14] S. Schumacher, A. Ruseckas, N. A. Montgomery, P. J. Skabara, A. L. Kanibolotsky, M. J. Paterson, I. Galbraith, G. A. Turnbull, I. D. W. Samuel, *J. Chem. Phys.* **2009**, 131, 154906.
- [15] E. Y. Choi, L. Mazur, L. Mager, M. Gwon, D. Pitrat, J. C. Mulatier, C. Monnereau, A. Fort, A. J. Attias, K. Dorkenoo, J. E. Kwon, Y. Xiao, K. Matczyszyn, M. Samoc, D.-W. Kim, A. Nakao, B. Heinrich, D. Hashizume, M. Uchiyama, S. Y. Park, F. Mathevet, T. Aoyama, C. Andraud, J. W. Wu, A. Barsella, J. C. Ribierre, *Phys. Chem. Chem. Phys.* **2014**, 16, 16941.
- [16] a) S. D. Lee, M. Sarmadi, F. Denes, J. L. Shohet, *Plasmas Polym.* **1997**, 2, 177; b) Z. Q. Hua, R. Sitaru, F. Denes, R. A. Young, *Plasmas Polym.* **1997**, 2, 199; c) H. Fujimoto, T. Miyayama, N. Sanada, C. Adachi, *Org. Electron.* **2013**, 14, 2994.
- [17] J. Kasprzak, M. Richard, S. Kundermann, A. Baas, P. Jeambrun, J. M. J. Keeling, F. M. Marchetti, M. H. Szymańska, R. André, J. L. Staehli, V. Savona, P. B. Littlewood, B. Deveaud, L. S. Dang, *Nature* **2006**, 443, 409.
- [18] D. N. Krizhanovskii, K. G. Lagoudakis, M. Wouters, B. Pietka, R. A. Bradley, K. Guda, D. M. Whittaker, M. S. Skolnick, B. Deveaud-Plédran, M. Richard, R. André, L. S. Dang, *Phys. Rev. B* **2009**, 80, 045317.
- [19] D. M. Coles, P. Michetti, C. Clark, W. C. Tsoi, A. M. Adawi, J.-S. Kim, D. G. Lidzey, *Adv. Funct. Mater.* **2011**, 21, 3691.
- [20] a) A. Baas, K. G. Lagoudakis, M. Richard, R. André, L. S. Dang, B. Deveaud-Plédran, *Phys. Rev. Lett.* **2008**, 100, 2; b) H. Ohadi, Y. Del Valle-Inclan Redondo, A. J. Ramsay, Z. Hatzopoulos, T. C. H. Liew, P. R. Eastham, P. G. Savvidis, J. J. Baumberg, *Phys. Rev. B* **2018**, 97, 1.